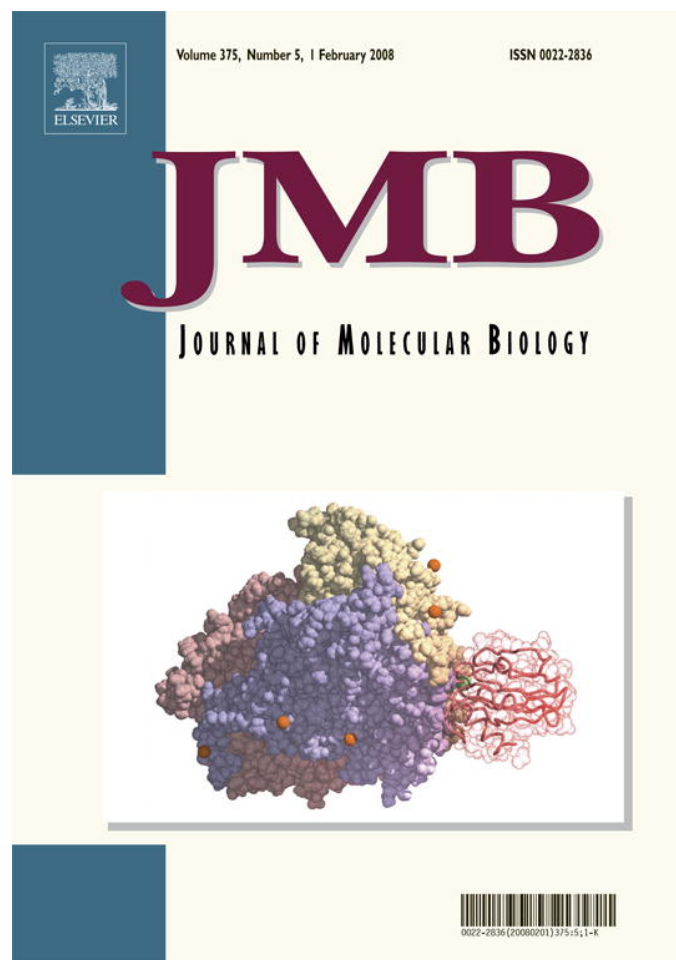


Provided for non-commercial research and education use.
Not for reproduction, distribution or commercial use.



This article was published in an Elsevier journal. The attached copy is furnished to the author for non-commercial research and education use, including for instruction at the author's institution, sharing with colleagues and providing to institution administration.

Other uses, including reproduction and distribution, or selling or licensing copies, or posting to personal, institutional or third party websites are prohibited.

In most cases authors are permitted to post their version of the article (e.g. in Word or Tex form) to their personal website or institutional repository. Authors requiring further information regarding Elsevier's archiving and manuscript policies are encouraged to visit:

<http://www.elsevier.com/copyright>

JMBAvailable online at www.sciencedirect.com ScienceDirect

Conformation of Pseudoazurin in the 152 kDa Electron Transfer Complex with Nitrite Reductase Determined by Paramagnetic NMR

Monica D. Vlasie, Rubén Fernández-Busnadiego, Miguel Prudêncio and Marcellus Ubbink*

Leiden University, Institute of Chemistry, Gorlaeus Laboratories, P.O. Box 9502 2300 RA Leiden The Netherlands

Received 2 August 2007; received in revised form 18 October 2007; accepted 16 November 2007 Available online 22 November 2007

Copper-containing nitrite reductase is able to catalyze the reduction of nitrite with a turnover rate of several hundreds per second. Electrons for the reaction are donated by the electron transfer protein pseudoazurin. The process of protein complex formation, electron transfer and dissociation must occur on the millisecond timescale to enable the fast turnover of the enzyme. The structure of this transient protein complex has been studied using paramagnetic NMR spectroscopy. Gadolinium complexes were attached specifically through two engineered Cys residues on three sites on the surface of nitrite reductase, causing strong distance-dependent relaxation effects on the residues of pseudoazurin. Docking of the two proteins based on these NMR-derived distance restraints and the chemical shift perturbation data shows convergence to a cluster of structures with an average root-mean-square deviation of 1.5 Å. The binding interface consists of polar and non-polar residues surrounded by charges. The interprotein distance between the two type-1 copper sites is 15.5(±0.5) Å, enabling fast interprotein electron transfer. The NMR-based lower limit estimate of 600 s⁻¹ for the dissociation rate constant and the fast electron transfer are consistent with the transient nature of the complex.

© 2007 Elsevier Ltd. All rights reserved.

Keywords: transient complex; electron transfer; denitrification; protein interactions; relaxation

Edited by A. G. Palmer III

Introduction

The first committed step in denitrification, the reduction of nitrite to gaseous nitric oxide is catalyzed by nitrite reductase (NiR). There are two types of NiR in the denitrifying bacteria; the multi-heme NiR and the multi-copper NiR. The copper-containing NiRs receive electrons from small blue copper proteins, azurin or pseudoazurin (Paz). Structures of copper-containing NiRs from different sources show that NiR consists of a homotrimer of about 110 kDa. Each subunit contains a type 1 copper atom buried at 7 Å underneath the surface, and a type 2 copper atom at the interface between

subunits. Electrons flow in from the blue copper protein to the type 1 copper atom and are transferred further to the type 2 copper atom in the active site.¹

In the denitrifying bacterium *Alcaligenes faecalis* S-6, Paz (14 kDa) acts as the physiological electron donor to a green copper-containing Nir.² Several studies on the sites of interaction between the two proteins have been reported. Mutagenesis and kinetic analysis demonstrated that the positively charged Paz residues such as Lys10, Lys38, Lys57 and Lys77 are important for binding to the negatively charged surface of Nir.^{3–6} A minimal binding interface on Paz was determined by NMR cross-saturation experiments showing a significant contribution of apolar residues to the complex formation.⁷ NMR chemical shift perturbations observed for Paz upon complex formation pointed towards a complex with a well-defined orientation. The perturbations were used in docking simulations, resulting in a model of the complex with an inter-

*Corresponding author. E-mail address: m.ubbink@chem.leidenuniv.nl.

Abbreviations used: NiR, nitrite reductase; ET, electron transfer; Paz, pseudoazurin; PRE, paramagnetic relaxation enhancement.

protein Cu–Cu distance of about 14 Å.⁸ Binding studies showed that three molecules of Paz can be bound per NiR trimer, with no evidence for cooperativity between sites.

X-ray crystallography is normally used for solving the structure of large macromolecules and their assemblies. However, it is difficult to obtain co-crystals of proteins that form complexes with low affinity. No crystal structure is available of the NiR–Paz complex, although disordered co-crystals have been reported.⁹

Recent advances in NMR, based on TROSY^{10,11} and perdeuteration,^{12–14} make solution studies of large proteins and macromolecular assemblies possible, as demonstrated by Wüthrich and co-workers on the GroES/GroEL complex (~900 kDa)¹⁵ and Kay and Sprangers on the 670 kDa 20 S proteasome.¹⁶

To determine the structure of the transient complex of NiR and Paz, we decided to use paramagnetic centers attached to NiR to provide long-range intermolecular distance information as experimental restraints in docking. In this way, there is no need for NMR assignment of the large NiR, because the smaller Paz is used to observe the intermolecular paramagnetic effects. To limit its mobility and to make it easier to model its location, a paramagnetic center was used that was attached *via* two arms to the protein surface.¹⁷ Previously, we have shown that such bidentate complexes of Gd can provide reliable distance information on the basis of paramagnetic relaxation effects in the range of 20–30 Å from the metal.^{18,19} Here, we show that by taking advantage of TROSY and perdeuteration, in combination with the use of paramagnetic NMR, an experimental structural model of the 152 kDa protein complex between NiR and Paz can be obtained. The results provide information about the nature of the interface and suggest paths for the interprotein electron transfer (ET).

Results and Discussion

Mapping the binding interface of the NiR–Paz complex

The copper in Paz was substituted for zinc (which mimics the oxidized form of the copper-containing protein) to avoid broadening of the Paz NMR spectrum by the paramagnetic Cu(II) and to avoid any intermolecular ET that might lead to effects other than those due to the binding. It has been shown that this substitution does not affect the structure significantly¹⁸ or influence the binding to Nir.²⁰ Attempts to determine a dissociation constant for the complex of NiR and Paz by NMR titration experiments have been hampered until now by the size of this complex.²⁰ A full titration of NiR into Zn–Paz was obtained using perdeuterated Paz in combination with TROSY. A global fit of the chemical shift differences between the bound and unbound forms of Paz for a few residues gave a K_d of 64(±8) μM (Figure 1), similar to the K_M value obtained for the NiR reaction under the same conditions ($K_M=77(±8)$ μM).²¹ Previous calorimetry studies yielded a K_d of ~160 μM for the Cu(II)–Paz binding to oxidized copper containing Nir.²⁰ The chemical shift perturbations indicate that complex formation is fast on the NMR timescale, with a $k_{off} \gg 600$ s⁻¹. This is consistent with the reported high turnover of NiR (k_{cat} forward ~1000 s⁻¹ at pH 6.5 and 25 °C).²¹ The large chemical shift perturbations observed for some of the residues suggest that this complex is found predominantly in a single orientation.^{22–24} Similar to previous studies on NiR–Paz interaction,^{7,8} the chemical shift map obtained for the complex indicates a binding site close to the exposed copper ligand, His81, which is expected to be involved in the interprotein ET (Figure 2).^{25–27}

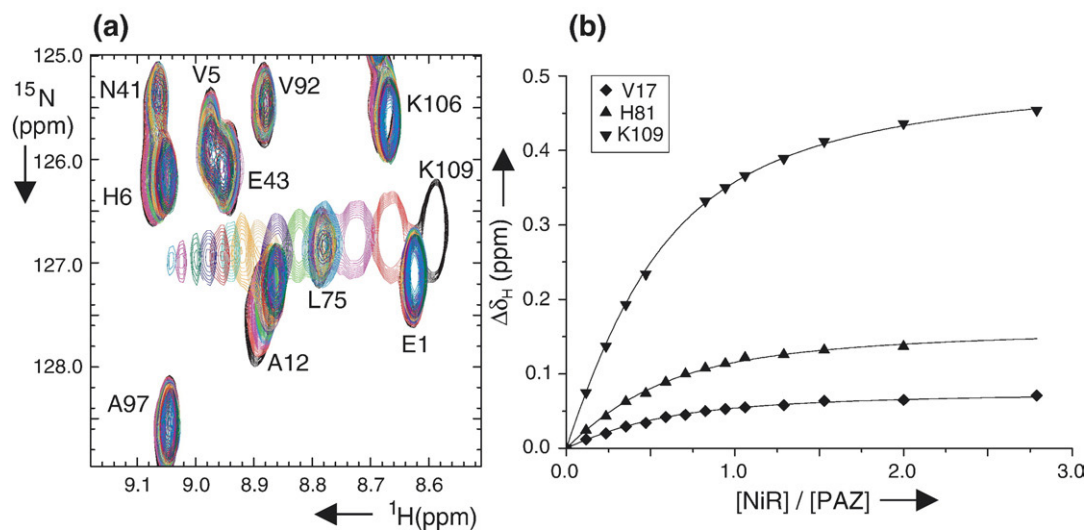


Figure 1. Titration of NiR to (²H,¹⁵N)-labeled Paz(Zn). (a) A region of the overlaid TROSY spectra, showing chemical shift perturbation for residue K109 in the titration of NiR to perdeuterated Paz(Zn) from 0 (black contours) to 2.8 equivalents of NiR (subunit concentration). (b) Amide proton chemical shift perturbations for several Paz residues. A global fit to a 1:1 binding model (continuous lines) yields $K_d=64(±8)$ μM.

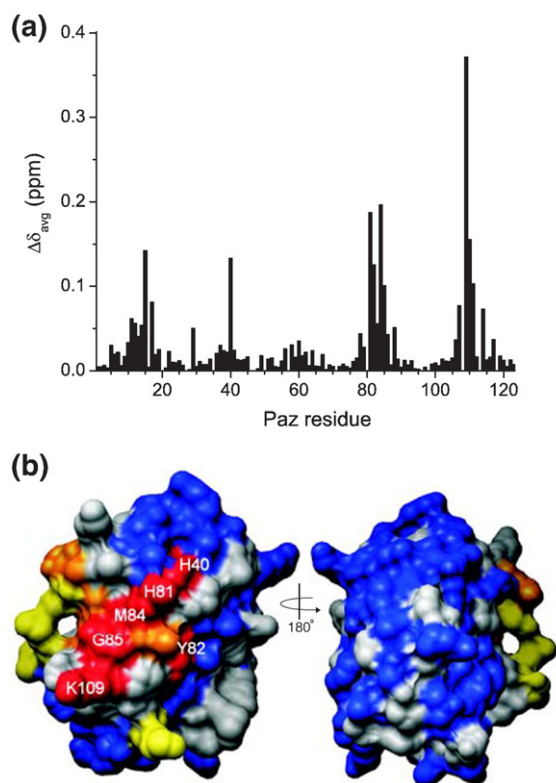


Figure 2. Map of the binding interface of Paz. (a) Change in the average chemical shift ($\Delta\delta_{\text{avg}}$) for Paz residues. (b) $\Delta\delta_{\text{avg}}$ is plotted onto a surface representation of Paz (PDB entry 3PAZ⁵³). Residues with $\Delta\delta_{\text{avg}} > 0.1$ ppm are depicted in red; > 0.05 ppm, orange; 0.04–0.05, yellow; and < 0.04 ppm, blue. Pro and unobserved residues are shown in grey.

Paramagnetic relaxation enhancement

To determine the orientation of Paz relative to NiR in the complex, paramagnetic probes were employed. By attaching a relaxation probe at a defined position on NiR, distances between the probe and Paz amides can be measured and used in the docking calculations as experimental distance restraints.²⁸

The lanthanide chelator CLaNP-1¹⁸ can be attached to two exposed Cys residues on proteins. Bidentate attachment ensures rigidity and makes it possible to model the position of the lanthanide ion relative to NiR within a few ångström units. Gadolinium-containing CLaNP was tested previously for its distance-dependence effects on a protein.¹⁹ A high degree of correlation was obtained between the distances derived from paramagnetic relaxation enhancements (PRE) and those from the crystal structure. Three surface-exposed double Cys mutants were engineered on NiR: N221C/A223C (NirA), T234C/A236C (NirB) and S333C/A336C (NirC), to serve as points of attachment of the paramagnetic probe. Wild-type (wt) NiR has no cysteine residue other than the buried ligand in the type 1 Cu site. The mutation sites for the attachment of the probe were chosen close to the proposed Paz binding site on Nir⁸ but far enough away to not

interfere with the binding of the two proteins. The chemical shift perturbation maps of Paz bound to the different mutants with the diamagnetic probe attached (CLaNP-1 containing yttrium, ^YCLaNP-1) were similar to that of the wild-type complex (data not shown), indicating that the probes bound to these positions do not modify the binding of NiR to Paz. The efficiency of binding the CLaNP molecule to the NiR mutants was checked by metal analysis. A ratio of gadolinium (or yttrium) to copper in NiR of 0.5 means that all the protein was labeled with the probe. For NirA, 50% labeling was obtained, 100% for NirB and 25% for NirC. It is not clear why labeling efficiency varies between the mutants, but these values were found in two independent labeling procedures of the mutants and were used in the calculation of the distance restraints (equations (3) in Materials and Methods). The values for the copper content of NiR obtained from the UV-vis spectra and those obtained from the metal analysis were compared and found to be the same for all the mutants analyzed, within a 10% error. This shows that copper is not lost from the protein during treatment with the reducing agent and probe attachment.

For measuring the PRE of the Paz amide protons, two samples were used, containing (²H,¹⁵N)-labeled Paz and an NiR mutant bound to either the paramagnetic ^{Gd}CLaNP or the diamagnetic ^YCLaNP. The intensity decrease due to the presence of the paramagnetic metal was determined. PREs were measured for different ratios of Paz and NiR. The ratio at which significant effects were observed on Paz, was used in the calculation of the distance restraints. The combined effect of chemical shift changes due to complex formation and broadening of the K109 peak due to the proximity of the Gd ion are shown in Figure 3(a) for NirA. The intensity loss due to PRE was measured for Paz resonances (Figure 3(b)) and mapped onto the crystal structure of the protein (Figure 3(c)).

Docking the NiR-Paz complex

To determine the orientation of Paz within the complex with NiR, docking calculations were performed on the basis of the two types of experimental information, chemical shift perturbations and PREs.

Chemical shift perturbations provide qualitative information about the distance between the residues of the two interacting proteins. It was assumed that the surface-exposed amides that show a $\Delta\delta_{\text{avg}} > 0.05$ ppm upon complex formation are part of the binding interface and therefore must be found in the proximity of residues of NiR. Residues with more than 40% surface accessibility were used in the calculation.²⁹

Peak broadening due to paramagnetic effects, R_2^{para} , was measured from the decrease in intensity of the peaks and the linewidth of the diamagnetic sample, using equation (2) and converted into distances using equations (3) as described in Material and Methods.

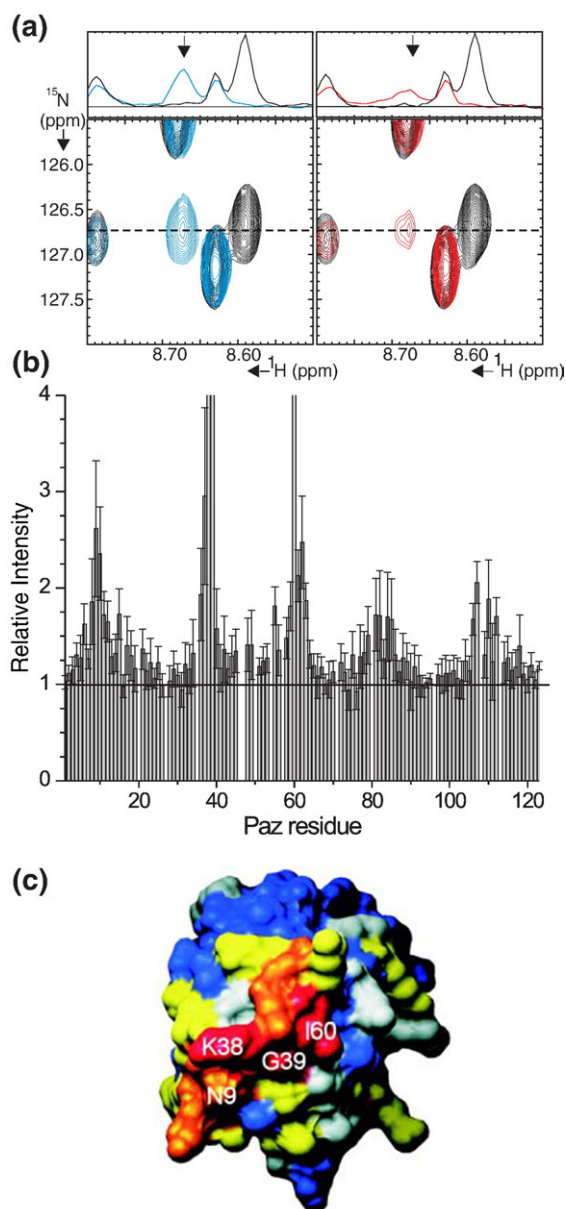


Figure 3. Paramagnetic relaxation enhancements. (a) Sections of the TROSY spectra of ($^2\text{H},^{15}\text{N}$)-labeled Paz in complex with 0.2 equivalent ^{15}N -labeled NirA (left, blue) or ^{15}N -labeled NirA (right, red), with free PAZ in black. The top panels show the slice through the ^1H dimension at the broken line. The arrow indicates the amide resonance of Lys109. (b) Intensity changes for Paz residues due to the relaxation effects of Gd^{3+} attached to NirA. Intensity ratios of the diamagnetic over the paramagnetic sample are plotted for all observed residues of Paz. (c) Map of the relaxation effects caused by Gd^{3+} attached to NirA onto Paz residues: residues broadened beyond detection, red; peak intensity decreased > twofold, orange; intensity decrease of 1.5-twofold, yellow; intensity decrease < 1.5-fold, are in blue. Pro and unobserved residues are shown in grey.

The crystal structures of Paz and NiR were used as rigid bodies in the docking calculations. NiR was kept fixed and Paz was allowed to move from ran-

dom positions and was driven by the distance-restraints energy term only. The van der Waals interactions were first constrained to the backbones and C^β atoms of the two proteins.

The possible effects from the paramagnetic probe attached to the adjacent subunits of NiR onto the residues of Paz interacting with one NiR subunit was taken into account by a sum averaging of the calculated distance from the Gd position on each monomer to the amide proton of Paz. Therefore, nine Gd atoms were built into the structure of NiR (for three different positions of the probe at each subunit in the trimer), although it is clear that only for NirA is the Gd from neighboring monomer close enough to exert an effect on Paz. Given that there are three equivalent docking sites on the NiR trimer, we have introduced an additional symmetry restraint to ensure that Paz docking is driven only towards one of the subunits of NiR (see Materials and Methods). When docking was performed with Gd atoms attached on only a single subunit, the structures showed a similar orientation but the minimum energy structures clustered with a much higher uncertainty and the calculated distances showed significantly higher violations (data not shown).

The total correlation time, τ_c , which is used in equation (3a) to calculate the distance restraints, is given by the combined contribution of the longitudinal electron relaxation time of Gd^{3+} (τ_s) and the rotational correlation time of the metal-proton vector (τ_r), with the smallest of the two contributing mostly to the total τ_c . From EPR studies, the electronic relaxation times of Gd(III)-DTPA were shown to be very long, in the low microsecond timescale³⁰ and therefore unlikely to be a major determinant of τ_c . For a 150 kDa complex, τ_r can be estimated from the Stokes equation to be around 50 ns (53 ns as determined with the program HYDRONMR³¹). Docking calculations of the two proteins, using the experimental distance restraints calculated with τ_c values varying from 5 ns to 200 ns, gave converging structures with different minimum energy levels (Figure 4, filled circles). The least violated set of restraints in the docked complex structure were calculated using a τ_c of 50–100 ns. A plot of the measured inter-protein Cu–Cu distance for the docked redox partners as a function of τ_c is shown in Figure 4 (open squares).

With the best 20 structures obtained with $\tau_c = 50$ ns, a short run of restrained rigid-body dynamics was performed, including all atoms. This was followed by energy minimization of the side-chains. Due to the side-chain interactions, Paz moved slightly away from the NiR. The final set of 20 structures has an average root-mean-square deviation (rmsd) from the mean structure of $1.5(\pm 0.5)$ Å for the backbone atoms, considering only the Paz molecules. The final structure of the complex between NiR and Paz is shown in Figure 5 based on the mean structure of the cluster.

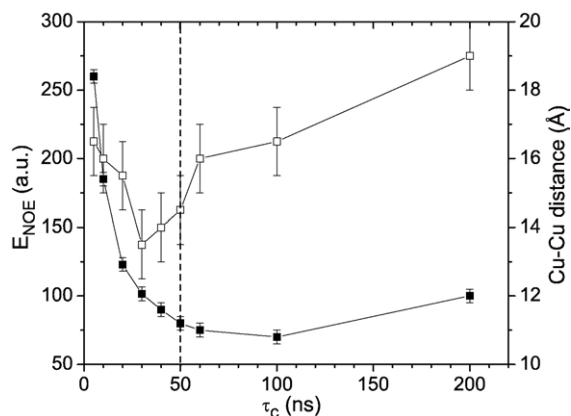


Figure 4. A plot of the low-energy structures obtained for different τ_c values (filled symbols, left-hand axis) with the error bars indicating the energy variation within the cluster of structures; and a plot of the donor (type 1 Cu in Paz) to acceptor (type 1 Cu in NiR) distance obtained at various rotational correlation times (open symbols, right-hand axis). The error bars indicate the variation within the cluster. The broken line marks the values of energy minimum and Cu–Cu distance for the 50 ns cluster used as the final docked structure. The continuous lines are to guide the eye.

Violation analysis

The correlation between the distances calculated from the PREs and those measured in the docked complex can be represented as in Figure 6, for each

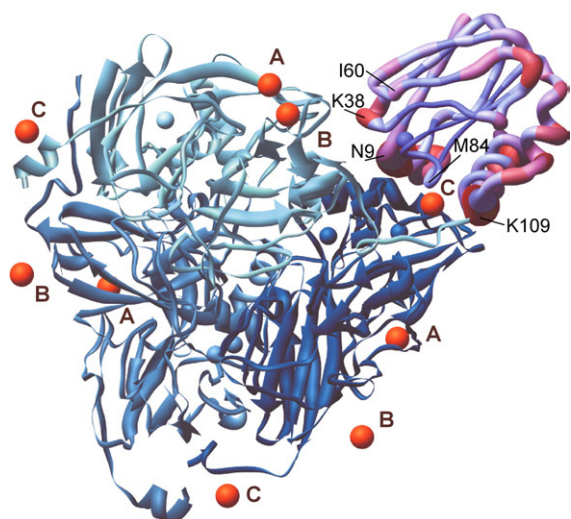


Figure 5. The structure of the complex. The NiR trimer is represented in ribbons with different shades of blue for each subunit. The Paz mean structure of the cluster is shown as a tube with the radius proportional to the average rmsd of each residue in the cluster and colored from blue to red from the smallest (0.59 Å) to the highest (2.28 Å) rmsd of the residues within the 20 structures. Some relevant residues are labeled. The copper ions of NiR and Paz are represented as blue spheres and the positions of the Gd ions for the three mutants of NiR are shown as orange spheres and labeled A, B and C for the positions of attachment in NirA, NirB and NirC, respectively.

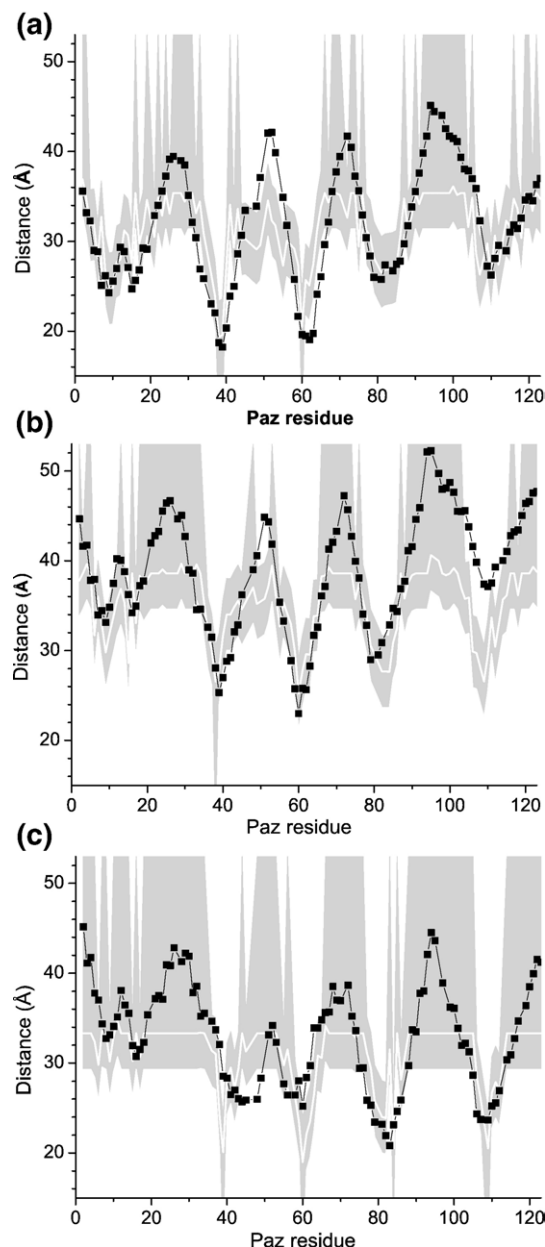


Figure 6. Violation analysis for the best structure in the cluster of the complex NiR-Paz. Comparison of the distances from the Gd atom in the paramagnetic probe attached to (a) NirA, (b) NirB (B) or (c) NirC to the Paz backbone amide protons, obtained from docking the two proteins with the PRE-derived distances. Distances in the calculated structure are indicated by filled symbols and the line. PRE-derived target distances are shown as continuous white lines and the bounds for the target distances as a shaded area.

set of probe positions. The experimental target distance is shown as a continuous white line and the boundaries as shaded areas. A distance restraint used in the docking is satisfied when the distance measured in the final complex (filled symbol) is within the shaded area. Analysis of the lowest-energy structure shows that the majority (77%, Table 1) of the restraints are satisfied. The average size of

Table 1. Violations of PRE restraints

	Violations			Total
	No. restraints	Upper bound	Lower bound	
NiRA	108	12 (3.2)	17 (2.6)	29 (27%)
NiRB	107	18 (3.4)	7 (0.6)	25 (23%)
NiRC	106	9 (2.4)	11 (2.1)	20 (19%)
Total	321	39 (3.0)	35 (1.8)	74 (23%)

The average size of the violation (in Å) is given in parentheses.

the violations is 2.6 Å, which is relatively small given the average target distance of 33 Å.

Lower bound violations are relatively modest (average 1.8 Å, Table 1) and observed mainly for NiRA and NiRC. These violations indicate that less paramagnetic relaxation was observed than predicted by the structure. This may be due to errors in the modeling, such as positioning to the gadolinium ions on NiR and the estimation of τ_c .

In two regions, around residue 52 in Figure 6(a) and residue 110 in Figure 6(b), the distances from the structure are significantly larger than those predicted by the NMR data. Similar observations have been made in other recent studies,^{28,32–34} and have been explained by assuming that such regions of the observed protein may be in close contact with the probe in other, minor conformations that represent the encounter state of the complex. The paramagnetic effect is strong at short distances and can result in significant line broadening even if the involved conformation represents only a small fraction of the complex. Compared to the data reported for the complex of cytochrome *c* and cytochrome *c* peroxidase,²⁸ few such violations are present, which suggests that Paz is found predominantly in one orientation within the complex. This is in accord with the size of the perturbations for the amide resonances of Paz upon complex formation, which classify as large ($\Delta\delta_{\text{avg}} > 0.4$ ppm for some residues at 100% bound proteins).²² Also, the affected residues form a clearly localized patch on the surface of Paz.

Residues at the interface

Figure 7 shows the residues of NiR and Paz that are within 5 Å of the other protein in the structure closest to the mean. In the NiR interface the non-polar and polar, uncharged residues that surround the type 1 copper ligand His145 are lined by negatively charged residues. Similarly, a ring of positively charged residues surrounds the small hydrophobic patch in the binding interface of Paz. Previous kinetic analysis of charge variants of both NiR and Paz have shown that the charged residues add to the affinity of the protein complex.^{3–6} It can be concluded that both charged and uncharged residues contribute to the binding of the two proteins^{7,8} with an interaction surface typical for ET complexes.^{22,35,36} The total solvent-accessible area buried at the interface of this complex is 1420 Å², in line with the expected interaction surface for transient complexes.^{37,38}

Electron transfer pathway

The k_{cat} of NiR is about 1000 s⁻¹ under the conditions described used in this study.²¹ To ensure such a high turnover of the enzyme, fast ET from Paz to NiR has to take place. The Cu–Cu distance between the two type 1 sites of the proteins was found to be 15.5(±0.5) Å for the complex of Cu(II)-Paz and oxidized NiR. The theoretical pathways³⁹ for electronic coupling for all the energy-minimized structures in the cluster were analyzed using the program HARLEM. Several possible routes were found within the 20 structures in the cluster of oxidized Paz with NiR. Of the two predominant structures, one involves two through-space jumps from the Paz Cu ligand His81 to NiR residue Met84,

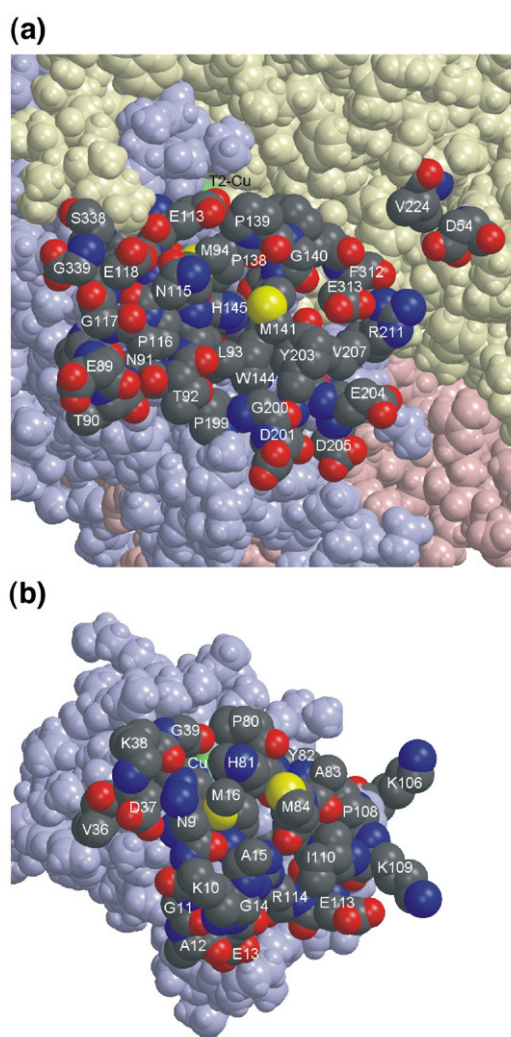


Figure 7. Binding interfaces for (a) NiR and (b) Paz. Residues with atoms within 5 Å of the partner protein in the structure of the complex that was closest to the mean structure are shown in CPK colors and are labeled. Other residues are in light blue, pink and green for the NiR subunits and in light blue for Paz. Copper atoms are in green. The NiR type 1 copper is located below His145 and is not visible. The orientations were obtained by +90° and -90° rotations of NiR and Paz relative to a side-view of the complex.

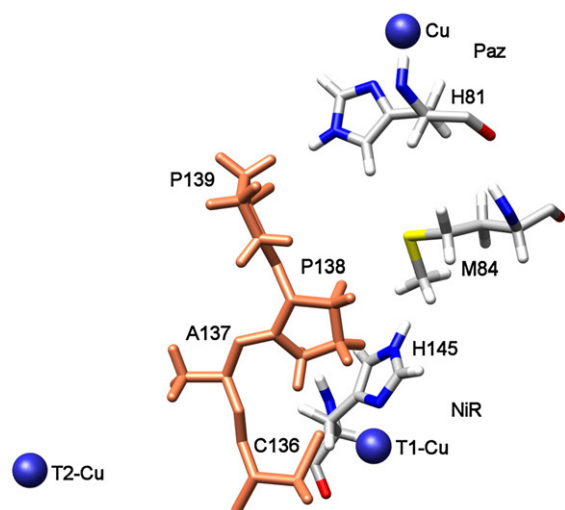


Figure 8. Dominant theoretical ET pathways between Paz and NiR type 1 copper centers. CPK colored sticks, coupling pathway involving two through-space jumps, ${}^{\text{Paz}}\text{His81}\text{-}{}^{\text{Paz}}\text{Met84}\text{-}{}^{\text{NiR}}\text{His145}$. Coral sticks, pathway involving ${}^{\text{Paz}}\text{His81}\text{-}{}^{\text{NiR}}\text{Pro139}\text{-}{}^{\text{NiR}}\text{Pro138}\text{-}{}^{\text{NiR}}\text{Ala137}\text{-}{}^{\text{NiR}}\text{Cys136}$.

and from Met84 to the NiR Cu ligand His145 (Figure 8). Alternatively, the coupling could comprise only one through-space jump between His81 of Paz and Pro139 of NiR. The residues involved in this path, besides the His81 copper ligand, are shown in coral in Figure 8. The relative coupling constants for the two pathways are similar, as judged by the Beratan and Onuchic approach. Dutton analysis⁴⁰ yields a value for intermolecular ET rate of $\approx 10^4 \text{ s}^{-1}$, using a reorganization energy for the two type 1 copper atoms of 0.7 eV,⁴¹ a midpoint potential difference of -0.05 V and a density (ρ) of 0.85. This indicates that intermolecular ET is not likely to be limiting the catalytic turn-over of NiR.

Theoretical docking and mutagenesis studies have shown that electronic coupling between copper-containing NiR and its physiological electron donor involves Trp138 and the surface-exposed Tyr197 of NiR.^{25,27} A three- to fourfold decrease in the rate of the interprotein ET was observed in Trp and Tyr mutants. In our study, the distance between the equivalent Tyr203 of NiR and His81, the exposed copper ligand in Paz, is about 7 Å and therefore less likely to be part of the path calculated for ET. As a note of caution, the theoretical pathways depend strongly on the precise position of the interface atoms and there is no experimental evidence in this study for the position of the side-chains of amino acid residues of the two interacting proteins.

Conclusions

Advances in NMR spectroscopy allow the study of large macromolecules. Here, we have performed NMR studies of a 152 kDa transient protein complex between nitrite reductase and pseudoazurin. Distance information defining the orientations of the

two proteins within the complex was derived from interprotein paramagnetic effects of Gd labels attached to NiR. Docking of the two proteins on the basis of these distance restraints and chemical shift perturbation data results in a cluster of low-energy structures with an average backbone rmsd of 1.5 Å. The resulting complex shows the features typical of a transient ET complex, with a moderately sized interface with only small non-polar areas centered around the exit/entry ports of the electron, surrounded by complementary charged residues. The resulting Cu–Cu distance allows for fast inter-protein ET.

Materials and Methods

Preparation of the labeled Paz

Isotopically enriched (${}^2\text{H}$, ${}^{15}\text{N}$)-labeled Paz was obtained by incubating *Escherichia coli* BL21(DE3) cells harboring the pET28a-based expression vector for the *A. faecalis* S-6 Paz gene¹⁸ in M9 minimal medium that contained ${}^{15}\text{NH}_4\text{Cl}$ (0.7 g/l) and $\text{d}_3\text{-acetate}$ (5 g/l). The deuteration of the protein was achieved by growing the cells in incremental percentages of deuterated media with the final culture being in about 80% ${}^2\text{H}_2\text{O}$.⁷ The purification of the copper-Paz was performed as described,¹⁹ and yielded about 50 mg of protein from 1 l of culture. Mass analysis of the purified Paz confirmed an 83% level of deuteration for the non-exchangeable hydrogen atoms in Paz ($m = 14350(\pm 2) \text{ Da}$). The concentration of copper-Paz was determined using an extinction coefficient at 596 nm of $2.9 \text{ mM}^{-1} \text{ cm}^{-1}$ and the purity was assessed by SDS-PAGE and isoelectric focusing gel electrophoresis in a pH range 3–9. The ratio of the absorbance at 278 nm and at 596 nm in Paz was 1.8, indicating a high-purity sample (>95%).²

Replacement of the Cu by Zn in Paz

To replace the Cu with Zn, the Paz solution was treated with potassium cyanide (100 mM dissolved in 0.5 M Tris–HCl, pH 7). In order to remove the CN^- and charge the protein with Zn, the solution was immediately loaded onto a desalting Superdex G-25 column equilibrated with 2 mM ZnCl_2 in 50 mM Tris–HCl, pH 7. The protein was eluted from the column with 50 mM Tris–HCl, pH 7. The fraction of the protein that was unfolded by the treatment, was removed by ion-exchange chromatography using a Q-Sepharose column equilibrated with 20 mM sodium phosphate, pH 6.5. The protein was eluted from this column with a salt gradient, at about 100 mM NaCl in the same buffer. The buffer was changed to 20 mM sodium phosphate (pH 6.5) and the protein was concentrated to 0.25 mM for the NMR experiments. The concentration of Paz(Zn) was determined using an extinction coefficient at 280 nm of $5.7 \text{ mM}^{-1} \text{ cm}^{-1}$.

Expression and purification of NiR

Three double-cysteine mutants of the *A. faecalis* S-6 NiR encoding gene in pET28a were prepared by site-directed mutagenesis using the QuikChange™ polymerase chain reaction (PCR) protocol from Stratagene. The primers

used were as follow: N221C/A223C (5'-CCG ACA CAT GTG GTG TTC TGC GGC TGT GTG GGC GC); T234C/A236C (5'-GGC GAC AAG GCC ATG TGC GCG TGC GTT GGC GAG AAA GTC C); S333C/A336C (5'-GG AAC GAC GAT CTG ATG ACG TGT GTT CTC TGC CCA TCT GG) with the desired mutation indicated in bold. All constructs were verified using restriction analysis and DNA sequencing. An additional silent mutation (in italics) in the first primer was introduced for easy identification of the mutant clones, due to the gain of an *Afl* III restriction site. For the second primer, a *Bgl* I site was lost by introduction of the mutation and, similarly, an *Afl* III site was gained for the third primer.

The wild-type and the mutant forms of NiR were produced and purified as described,⁸ yielding 200–300 mg of protein/l of culture. The concentration of protein was determined using an extinction coefficient at 460 nm of 2.9 mM⁻¹ cm⁻¹ per subunit.

Attachment of the paramagnetic probes to NiR

Synthesis of the CLaNP-1 molecule has been described.¹⁸ To attach the probe to the two engineered Cys residues, NiR was first treated with β -mercaptoethanol (20 mM final concentration) to remove possible protein dimers by reduction of disulphide bonds. After incubation at room temperature for 30 min, the protein was loaded onto a desalting Superdex G-25 column equilibrated with a degassed solution of 20 mM sodium phosphate (pH 7) to remove the reductant. Immediately after elution, two molar equivalents of the probe to the NiR subunit were added and the solution was stirred overnight at 4 °C under semi-anaerobic conditions. The protein was then loaded onto a Sephacryl S-200 high-resolution (Pharmacia) gel-filtration column and eluted in 20 mM sodium phosphate (pH 7), 150 mM NaCl. Finally, the protein was concentrated and the buffer was replaced with 20 mM sodium phosphate (pH 6.5) for use in NMR experiments.

Quantification of the CLaNP molecule bound to NiR was performed by metal analysis (atomic flame-ionization spectroscopy) of the amount of Gd³⁺ or Y³⁺ in the sample, relative to the copper content. A ratio of 1:2 for Gd³⁺ (Y³⁺)/Cu indicates 100% probe bound to the NiR molecule. The copper content obtained from metal analysis was found to be almost twice as high as the copper measured by UV-vis spectroscopy, in which only the type 1 copper can be observed. This indicates that the more labile type 2 copper is not lost during the treatment with the reductant agent.

NMR spectroscopy

The NMR samples of (²H,¹⁵N)-labeled Zn-Paz (~250 μ M) were prepared as described above in phosphate buffer (pH 6.5) with 6% (v/v) ²H₂O added for lock. NiR of wild-type or CLaNP-labeled variants was prepared in the same buffer at a concentration of 1–3 mM and microliter aliquots of the stock solution were used in the NMR titration experiments. For the binding interface mapping, up to three equivalents of wild-type NiR (subunit concentration) were titrated into the Paz solution. For the PRE measurements, two sets of samples were used for each addition of NiR into Paz: one containing the paramagnetic Gd³⁺-CLaNP bound to NiR and one containing the diamagnetic Y³⁺-CLaNP bound to NiR, as a control sample. Calculation of the distance restraints was based on the samples with 0.38 equivalent of NiR to Paz for NirA, 0.32 equivalent for NirB and 0.53 equivalent for NirC. The ¹⁵N-¹H TROSY spectra¹¹ were acquired at

14.1 T on a Bruker DMX600 spectrometer equipped with a TXI-Z-GRAD (¹H,¹³C and ¹⁵N) probe operating at 298 K. Data processing was done with AZARA software† and analyzed with Ansig for Windows.⁴² The assignments of the ¹⁵N-Zn-Paz HSQC spectra were taken from the literature.^{18,43}

Chemical shift perturbation analysis

The chemical shift perturbations of several amide ¹H nuclei were plotted against the molar ratio of NiR and Paz. The data for these residues were fit globally in OriginPro 7.5 (OriginLab Corp., Northampton, MA) using a 1:1 (Paz/NiR subunit) binding model that takes in consideration the dilution effects to yield the dissociation constant of the complex.²⁴ The chemical shift perturbations were extrapolated to 100%, and the average chemical shift perturbation of the ¹⁵N and ¹H nuclei for a given amide was calculated using:⁴⁴

$$\Delta\delta_{\text{avg}} = (0.5(\Delta\delta_{\text{N}}/5)^2 + 0.5(\Delta\delta_{\text{H}})^2)^{0.5} \quad (1)$$

in which $\Delta\delta_{\text{N}}$ and $\Delta\delta_{\text{H}}$ represent the perturbation of the chemical shift of the amide nitrogen and proton upon protein binding, respectively.

Paramagnetic relaxation enhancement

The broadening of the Paz amide resonances caused by the paramagnetic Gd ion attached to NiR was analyzed as described.¹⁹ Briefly, the intensity ratio of the amide resonances of the paramagnetic and diamagnetic form of the protein complex can be related to the paramagnetic contribution of the transverse ¹H relaxation, R_2^{para} , according to equation (2),⁴⁵ assuming that the contribution to the ¹⁵N relaxation can be neglected.

$$\frac{I^{\text{para}}}{I^{\text{dia}}} = \frac{R_2^{\text{dia}} \exp(-R_2^{\text{para}} t)}{R_2^{\text{dia}} + R_2^{\text{para}}} \quad (2)$$

where I^{para} and I^{dia} are the peak intensities for an amide resonance in the paramagnetic and diamagnetic sample, respectively; R_2^{dia} represents the intrinsic ¹H transverse relaxation rate, and t is the total INEPT evolution time (9 ms). R_2^{dia} is derived from the linewidths ($\Delta\nu_{1/2}$) of the resonances of the diamagnetic sample ($R_2^{\text{dia}} = \pi\Delta\nu_{1/2}$). To obtain $\Delta\nu_{1/2}$, the program MestRec‡ was used for fitting ¹H resonance traces from the TROSY spectra of the Paz-¹⁵N CLaNP NiR complexes. The R_2^{para} values were converted into distances using equations (3), which is a simplified version of the Solomon-Bloembergen equation.⁴⁶

$$r = \sqrt[6]{C \frac{K}{R_2^{\text{para}}} \left(4\tau_c + \frac{3\tau_c}{1 + \omega_H^2 \tau_c^2} \right)} \quad (3a)$$

where r is the lanthanide–amide proton distance, ω_H is the Larmor frequency of the proton spin, and τ_c is the correlation time.

A value of 25.83×10^{-32} cm⁶ s⁻² was used for K , which is defined as:

$$K = \frac{1}{15} \left(\frac{\mu_0}{4\pi} \right)^2 \gamma_H^2 g^2 \mu_B^2 J(J+1) \quad (3b)$$

† <http://www.bio.cam.ac.uk/azara>

‡ <http://www.mestrec.com>

where μ_0 is the vacuum permeability, γ_H is the proton gyromagnetic ratio, μ_B is the Bohr magneton, g is the electronic g factor and J is the quantum number for the Gd (7/2).⁴⁷

The constant C is the product of the fraction of bound lanthanide per NiR monomer, and the fraction bound NiR to Paz.

Recently, the potential artefacts of the method used in this study to determine R_2^{para} were discussed.⁴⁸ For the NiR-Paz complex, the errors introduced are relatively small, because τ_c is large (50–100 ns) and dominated by τ_r . Consequently, Curie relaxation is negligible and underestimation of R_2^{para} is limited. The paramagnetic effects are intermolecular, so partial labeling results in proportional decrease of the paramagnetic effects, which is compensated for in constant C . Any artifacts are most severe for nuclei with large R_2^{para} values, but the use of classes of distance restraints (see below) makes the docking result insensitive to errors in the distance estimates for those nuclei. A two-point experiment was reported to derive R_2 values more directly.⁴⁸ Though less prone to artefacts in principle, in our hands this approach yielded similar values for R_2^{para} but with lower precision due to significant larger signal loss in this experiment.

PRE restraints

The calculated distances were divided into three classes of restraints. The first class comprised the residues for which the intensity of the amide resonances was affected > fivefold and those for which resonances were broadened beyond detection. These residues were considered to be too close to the paramagnetic center for a lower bound to be set. The target distance was calculated using equations (3). For resonances that were broadened beyond detection, the noise level was used to determine an upper limit of the intensity ratio (equation (2)). The upper bound was set to the calculated distance +4 Å. The second class contained the residues for which the intensity of the amide resonances was affected < fivefold but > 1.2-fold. For these residues, an upper and a lower bound of 4 Å was given to the distances calculated above. The third class comprised the residues for which the peak intensity was decreased < 1.-fold, and these residues were considered to be too far away to be affected by the paramagnetic probe. An upper value of 5 Hz was estimated for R_2^{para} for these residues. With equations (2) and (3), this value was converted into a target distance. Only a lower limit bound of the distance -4 Å was set for this class.

Interface restraints

The accessible surface area (ASA) for nuclei that showed more than 0.05 ppm shift for the $\Delta\delta_{\text{avg}}$ was calculated with NACCESS 2.1.1.⁴⁹ For residues in which ASA was at least 40%, it was considered that the chemical shift is due to the change in the environment at the protein-protein interface and therefore these Paz residues must be within a certain distance from the NiR. The interface restraints were set up as distance restraints by r^{-6} averaging of all distances from the amide proton of the perturbed residue in Paz to all 166 backbone amide nitrogen atoms in NiR that are found within 20 Å from the type 1 Cu center in the NiR subunit where Paz docks. A value of 13(±5) Å was set for the target of the square-well function.⁵⁰

The number of distance restraints derived from the relaxation and chemical shift perturbation experiments and the scaling factors used in the docking of the two proteins are given in Table 2. The scales were chosen to

Table 2. Number of distance restraints used in the Xplor-NIH docking

Class of restraints	No. restraints	Scale	Relative contribution
NMR relaxation	324	1	324
Chemical shift interface restraints	5	30	150

give the PRE data about twice the weight of the chemical shift interface restraints.

An additional symmetry distance restraint was added to drive the docking of one molecule of Paz towards one of the three equivalent subunits of NiR. The restraint was satisfied once the type 1 copper centers of Paz and subunit C of NiR were closer than 25 Å.

Docking

Restrained rigid-body molecular dynamics and restrained energy minimization of the side-chains were performed in X-PLOR-NIH version 2.9.9.⁵¹ The crystal structures of *A. faecalis* NiR and Paz (PDB entry codes 1SJM⁵² and 3PAZ⁵³) were used as the starting structures in the docking of the two proteins. Protons were added and an initial energy minimization of the side-chain atoms was performed on the proteins before docking. Also, the Gd atoms were built onto the NiR structure by patching the known structure of the CLaNP molecule¹⁸ at all three positions engineered in the protein and for all three monomers of the protein. In this way, nine Gd atoms were added. The orientations of the probe and several residues in the vicinity were optimized by Powell energy minimization.

In the rigid-body molecular dynamics used for the docking of the two proteins, only the energy terms from the distance restraints and the van der Waals repulsion were used. In this step, the interaction between the two proteins was restricted to the backbone and C^β atoms of both Paz and NiR. Powell gradient energy minimization was applied afterwards to the annealed structures, keeping the backbone atoms fixed and allowing only the side-chains to move using the bond, angle, dihedral, improper and van der Waals energy terms to generate the final structures of the complex.

Calculations of the best pathway for the ET between the type 1 copper centers of the two proteins were performed with the program HARLEM⁵.³⁹ Molecular surfaces shown in the Figures were produced using UCSF Chimera⁵⁴ and Figure 7 was drawn using MOLSCRIPT⁵⁵ and Raster3D.⁵⁶

Protein Data Bank accession numbers

The best 20 structures have been deposited at the PDB under entry 2P80.

Acknowledgements

Dr A. N. Volkov is acknowledged for his help with the docking calculations. This work was supported

§ http://kurnikovcluster01.eoh.pitt.edu/~igor/harlem_main.html

by the Netherlands Organisation for Scientific Research (NWO), VIDI grant 700.52.425. R.F.B. was supported by the "MagRes" Marie Curie Training Site, contract no HPMT-CT-2000-00120.

Supplementary Data

Supplementary data associated with this article can be found, in the online version, at doi:10.1016/j.jmb.2007.11.056

References

- Adman, E. T. & Murphy, M. E. P. (2001). Copper nitrite reductase. In *Handbook of Metalloproteins* (Messerschmidt, A., Huber, R., Poulos, T. L., Wieghardt, K., Cygler, M. & Bode, W., eds), pp. 1381–1390, John Wiley & Sons, New York.
- Kakutani, T., Watanabe, H., Arima, K. & Beppu, T. (1981). A blue protein as an inactivating factor for nitrite reductase from *Alcaligenes faecalis* strain S-6. *J. Biochem. (Tokyo)*, **89**, 463–472.
- Kataoka, K., Yamaguchi, K., Kobayashi, M., Mori, T., Bokui, N. & Suzuki, S. (2004). Structure-based engineering of *Alcaligenes xylosoxidans* copper-containing nitrite reductase enhances intermolecular electron transfer reaction with pseudoazurin. *J. Biol. Chem.* **279**, 53374–53378.
- Kukimoto, M., Nishiyama, M., Ohnuki, T., Turley, S., Adman, E. T., Horinouchi, S. & Beppu, T. (1995). Identification of interaction site of pseudoazurin with its redox partner, copper-containing nitrite reductase from *Alcaligenes faecalis* S-6. *Prot. Engin.* **8**, 153–158.
- Kukimoto, M., Nishiyama, M., Tanokura, M., Murphy, M. E. P., Adman, E. T. & Horinouchi, S. (1996). Site-directed mutagenesis of azurin from *Pseudomonas aeruginosa* enhances the formation of an electron-transfer complex with a copper-containing nitrite reductase from *Alcaligenes faecalis* S-6. *FEBS Letters*, **394**, 87–90.
- Kukimoto, M., Nishiyama, M., Tanokura, M., Adman, E. T. & Horinouchi, S. (1996). Studies on protein-protein interaction between copper-containing nitrite reductase and pseudoazurin from *Alcaligenes faecalis* S-6. *J. Biol. Chem.* **271**, 13680–13683.
- Impagliazzo, A. & Ubbink, M. (2004). Mapping of the binding site on pseudoazurin in the transient 152 kDa complex with nitrite reductase. *J. Am. Chem. Soc.* **126**, 5658–5659.
- Impagliazzo, A., Krippahl, L. & Ubbink, M. (2005). Pseudoazurin-nitrite reductase interactions. *Chembiochem*, **6**, 1648–1653.
- Murphy, M. E. P., Turley, S. & Adman, E. T. (1998). On the mechanism of nitrite reductase: complex between pseudoazurin and nitrite reductase from *A. cycloclastes*. In *Biological Electron Transfer Chains: Genetics, Composition and Mode of Operation* (Canthers, G. W. & Vijgenboom, E., eds), pp. 115–128, Kluwer Academic Publishers, Dordrecht, The Netherlands.
- Riek, R., Wider, G., Pervushin, K. & Wüthrich, K. (1999). Polarization transfer by cross-correlated relaxation in solution NMR with very large molecules. *Proc. Natl Acad. Sci. USA*, **96**, 4918–4923.
- Pervushin, K., Riek, R., Wider, G. & Wüthrich, K. (1997). Attenuated T2 relaxation by mutual cancellation of dipole-dipole coupling and chemical shift anisotropy indicates an avenue to NMR structures of very large biological macromolecules in solution. *Proc. Natl Acad. Sci. USA*, **94**, 12366–12371.
- Fiaux, J., Bertelsen, E. B., Horwich, A. L. & Wüthrich, K. (2004). Uniform and residue-specific N-15-labeling of proteins on a highly deuterated background. *J. Biomol. NMR*, **29**, 289–297.
- Sattler, M. & Fesik, S. W. (1996). Use of deuterium labeling in NMR: Overcoming a sizeable problem. *Structure*, **4**, 1245–1249.
- Venters, R. A., Farmer, B. T., II, Fierke, C. A. & Spicer, L. D. (1996). Characterizing the use of perdeuteration in NMR studies of large proteins: ¹³C, ¹⁵N and ¹H assignments of human carbonic anhydrase II. *J. Mol. Biol.* **264**, 1101–1116.
- Fiaux, J., Bertelsen, E. B., Horwich, A. L. & Wüthrich, K. (2002). NMR analysis of a 900 K GroEL-GroES complex. *Nature*, **418**, 207–211.
- Sprangers, R. & Kay, L. E. (2007). Quantitative dynamics and binding studies of the 20S proteasome by NMR. *Nature*, **445**, 618–622.
- Keizers, P. H. J., Desreux, J. F., Overhand, M. & Ubbink, M. (2007). Increased paramagnetic effect of a lanthanide protein probe by two-point attachment. *J. Am. Chem. Soc.* **129**, 9292–9293.
- Prudêncio, M., Rohovec, J., Peters, J. A., Tocheva, E., Boulanger, M. J., Murphy, M. E. P. et al. (2004). A caged lanthanide complex as a paramagnetic shift agent for protein NMR. *Chem. Eur. J.* **10**, 3252–3260.
- Vlasie, M. D., Comuzzi, C., van den Nieuwendijk, A. M. C. H., Prudêncio, M., Overhand, M. & Ubbink, M. (2007). Long-range distance NMR effects in a protein labeled with a lanthanide-DOTA chelate. *Chem. Eur. J.* **13**, 1715–1723.
- Impagliazzo, A., Blok, A. J., Cliff, M. J., Ladbury, J. E. & Ubbink, M. (2007). Redox-state-dependent complex formation between pseudoazurin and nitrite reductase. *J. Am. Chem. Soc.* **129**, 226–233.
- Wijma, H. J., Canters, G. W., de Vries, S. & Verbeet, M. P. (2004). Bidirectional catalysis by copper-containing nitrite reductase. *Biochemistry*, **43**, 10467–10474.
- Prudêncio, M. & Ubbink, M. (2004). Transient complexes of redox proteins: structural and dynamic details from NMR studies. *J. Mol. Recogn.* **17**, 524–539.
- Worrall, J. A. R., Liu, Y., Crowley, P. B., Nocek, J. M., Hoffman, B. M. & Ubbink, M. (2002). Myoglobin and cytochrome *b₅*: a nuclear magnetic resonance study of a highly dynamic protein complex. *Biochemistry*, **41**, 11721–11730.
- Worrall, J. A. R., Reinle, W., Bernhardt, R. & Ubbink, M. (2003). Transient protein interactions studied by NMR spectroscopy: the case of cytochrome *c* and adrenodoxin. *Biochemistry*, **42**, 7068–7076.
- Barrett, M. L., Harris, R. L., Antonyuk, S., Hough, M. A., Ellis, M. J., Sawers, G. et al. (2004). Insights into redox partner interactions and substrate binding in nitrite reductase from *Alcaligenes xylosoxidans*: crystal structures of the Trp138His and His313Gln mutants. *Biochemistry*, **43**, 16311–16319.
- Murphy, L. M., Dodd, F. E., Yousafzai, F. K., Eady, R. R. & Hasnain, S. S. (2002). Electron donation between copper containing nitrite reductases and cupredoxins: the nature of protein-protein interaction in complex formation. *J. Mol. Biol.* **315**, 859–871.
- Yamaguchi, K., Shuta, K. & Suzuki, S. (2005). Roles of Trp144 and Tyr203 in copper-containing nitrite reductase from *Achromobacter cycloclastes* IAM1013. *Biochem. Biophys. Res. Commun.* **336**, 210–214.

28. Volkov, A. N., Worrall, J. A. R., Holtzmann, E. & Ubbink, M. (2006). Solution structure and dynamics of the complex between cytochrome *c* and cytochrome *c* peroxidase determined by paramagnetic NMR. *Proc. Natl Acad. Sci. USA*, **103**, 18945–18950.
29. de Vries, S. J., van Dijk, A. D. J. & Bonvin, A. M. J. J. (2006). WHISCY: What information does surface conservation yield? Application to data-driven docking. *Proteins: Struct. Funct. Bioinformatics*, **63**, 479–489.
30. Caravan, P., Ellison, J. J., McMurry, T. J. & Lauffer, R. B. (1999). Gadolinium(III) chelates as MRI contrast agents: structure, dynamics, and applications. *Chem. Rev.* **99**, 2293–2352.
31. Garcia de la Torre, J. G., Huertas, M. L. & Carrasco, B. (2000). HYDRONMR: prediction of NMR relaxation of globular proteins from atomic-level structures and hydrodynamic calculations. *J. Magn. Reson.* **147**, 138–146.
32. Iwahara, J., Zweckstetter, M. & Clore, G. M. (2006). NMR structural and kinetic characterization of a homeodomain diffusing and hopping on nonspecific DNA. *Proc. Natl Acad. Sci. USA*, **103**, 15062–15067.
33. Iwahara, J. & Clore, G. M. (2006). Detecting transient intermediates in macromolecular binding by paramagnetic NMR. *Nature*, **440**, 1227–1230.
34. Tang, C., Iwahara, J. & Clore, G. M. (2006). Visualization of transient encounter complexes in protein-protein association. *Nature*, **444**, 383–386.
35. Xu, X., Kim, S. K., Schürmann, P., Hirasawa, M., Tripathy, J. N., Smith, J. *et al.* (2006). Ferredoxin/ferredoxin-thioredoxin reductase complex: Complete NMR mapping of the interaction site on ferredoxin by gallium substitution. *FEBS Letters*, **580**, 6714–6720.
36. Crowley, P. B. & Carrondo, M. A. (2004). The architecture of the binding site in redox protein complexes: Implications for fast dissociation. *Proteins: Struct. Funct. Bioinformatics*, **55**, 603–612.
37. Jones, S. & Thornton, J. M. (1996). Principles of protein-protein interactions. *Proc. Natl Acad. Sci. USA*, **93**, 13–20.
38. Díaz-Moreno, I., Díaz-Quintana, A., De la Rosa, M. A. & Ubbink, M. (2005). Structure of the complex between plastocyanin and cytochrome *f* from the cyanobacterium *Nostoc* sp. PCC 7119 as determined by paramagnetic NMR. The balance between electrostatic and hydrophobic interactions within the transient complex determines the relative orientation of the two proteins. *J. Biol. Chem.* **280**, 18908–18915.
39. Onuchic, J. N., Beratan, D. N., Winkler, J. R. & Gray, H. B. (1992). Pathway analysis of protein electron-transfer reactions. *Annu. Rev. Biophys. Biomol. Struct.* **21**, 349–377.
40. Page, C. C., Moser, C. C., Chen, X. & Dutton, P. L. (1999). Natural engineering principles of electron tunnelling in biological oxidation-reduction. *Nature*, **402**, 47–52.
41. Cascella, M., Magistrato, A., Tavernelli, I., Carloni, P. & Rothlisberger, U. (2006). Role of protein frame and solvent for the redox properties of azurin from *Pseudomonas aeruginosa*. *Proc. Natl Acad. Sci. USA*, **103**, 19641–19646.
42. Helgstrand, M., Kraulis, P., Allard, P. & Härd, T. (2000). Ansig for Windows: an interactive computer program for semiautomatic assignment of protein NMR spectra. *J. Biomol. NMR*, **18**, 329–336.
43. Impagliazzo, A. & Ubbink, M. (2004). ^1H , ^{13}C and ^{15}N resonance assignment of Cu(I)-pseudoazurin from *Alcaligenes faecalis* S-6. *J. Biomol. NMR*, **29**, 541–542.
44. Grzesiek, S., Bax, A., Clore, G. M., Gronenborn, A. M., Hu, J. S., Kaufman, J. *et al.* (1996). The solution structure of HIV-1 Nef reveals an unexpected fold and permits delineation of the binding surface for the SH3 domain of Hck tyrosine protein kinase. *Nature Struct. Biol.* **3**, 340–345.
45. Battiste, J. L. & Wagner, G. (2000). Utilization of site-directed spin labeling and high-resolution heteronuclear nuclear magnetic resonance for global fold determination of large proteins with limited nuclear overhauser effect data. *Biochemistry*, **39**, 5355–5365.
46. Banci, L., Bertini, I. & Luchinat, C. (1991). *Nuclear and Electron Relaxation the Magnetic Nucleus-Unpaired Electron Coupling in Solution*, VCH, New York, NY.
47. Bertini, I., Luchinat, C., Parigi, G. & Pierattelli, R. (2005). NMR spectroscopy of paramagnetic metalloproteins. *ChemBiochem*, **6**, 1536–1549.
48. Iwahara, J., Tang, C. & Clore, G. M. (2007). Practical aspects of H-1 transverse paramagnetic relaxation enhancement measurements on macromolecules. *J. Magn. Reson.* **184**, 185–195.
49. Gerstein, M. (1992). A resolution-sensitive procedure for comparing protein surfaces and its application to the comparison of antigen-combining sites. *Acta Crystallog. sect. A*, **48**, 271–276.
50. Ubbink, M., Ejdebäck, M., Karlsson, B. G. & Bendall, D. S. (1998). The structure of the complex of plastocyanin and cytochrome *f*, determined by paramagnetic NMR and restrained rigid-body molecular dynamics. *Structure*, **6**, 323–335.
51. Schwieters, C. D., Kuszewski, J. J., Tjandra, N. & Clore, G. M. (2003). The Xplor-NIH NMR molecular structure determination package. *J. Magn. Reson.* **160**, 65–73.
52. Tocheva, E. I., Rosell, F. I., Mauk, A. G. & Murphy, M. E. P. (2004). Side-on copper-nitrosyl coordination by nitrite reductase. *Science*, **304**, 867–870.
53. Libeu, C. A. P., Kukimoto, M., Nishiyama, M., Horinouchi, S. & Adman, E. T. (1997). Site-directed mutants of pseudoazurin: explanation of increased redox potentials from X-ray structures and from calculation of redox potential differences. *Biochemistry*, **36**, 13160–13179.
54. Pettersen, E. F., Goddard, T. D., Huang, C. C., Couch, G. S., Greenblatt, D. M., Meng, E. C. & Ferrin, T. E. (2004). UCSF chimera — a visualization system for exploratory research and analysis. *J. Comput. Chem.* **25**, 1605–1612.
55. Kraulis, P. J. (1991). MOLSCRIPT: a program to produce both detailed and schematic plots of protein structures. *J. Appl. Crystallog.* **24**, 946–950.
56. Merrit, E. A. & Bacon, D. J. (1997). Raster3D photo-realistic molecular graphics. *Methods Enzymol.* **277**, 505–524.